Thickness effect of NACA symmetric hydrofoils on hydrodynamic behavior and boundary layer states

Henda Djeridi, Christophe Sarraf, Jean-Yves Billard

Thickness Effect of NACA Symmetric Hydrofoils on Hydrodynamic Behaviour and Boundary Layer States

H. Djeridi, C. Sarraf, and J.Y. Billard

Abstract The present study investigates experimentally the hydrodynamic behavior of 2D NACA (15%, 25%, 35%) symmetric hydrofoils at Reynolds number range $0.5 \cdot 10^5$ to $1.3 \cdot 10^6$. A particular attention is paid on the hysteretic behavior at static stall angle and a detailed cartography of boundary layer structures (*integral quantities and velocity profiles*) is given in order to put in evidence the mechanism of the detachment and the onset of von Karman instability.

Keywords Lift and drag · Thick foils · Boundary layer · Von Karman street

1 Introduction

In the context of podded propulsion, thick foils are used in naval shipyards to develop fins, rudders or POD Struts. One of the main interest of these thick hydrofoils is the stall delay that such profiles can provide when used at high angle of attack. In spite of their increasing use their behavior is not clearly understood and very few data are available concerning the hydrodynamic behavior at low and high incidences and also concerning the *turbulent boundary layer structures, performance control, unsteady separated flows and vibrations*. The effect of the thickness that leads to a surprising increase of the lift coefficient has been studied by Thwaites [1]. This effect can be observed for moderate thicknesses and the threshold value of the thickness above what this effect is observed is not clear. Some studies have been devoted to thickness effects on global parameters but few of them have investigated the detail of the flow in the boundary layer with adverse pressure gradient. The present work intends to clarify this point.

H. Djeridi (✉)
Laboratoire de Physique des Océans (LPO, UMR 6523), UFR Sciences et Techniques, 6 Avenue le Gorgeu, C.S. 93837, 29238 Brest Cedex 3, France
e-mail: Henda.djeridi@univ-brest.fr

C. Sarraf and J.Y. Billard
Institut de Recherche de l'Ecole Navale (IRENav, EA 3634), Ecole Navale BP 600, Lanvéoc Poulmic, 29240 BREST ARMEES France

If numerous works have focus on flat plates boundary layers with or without adverse pressure gradients [2–4] very few have been presented concerning boundary layers on foils and particularly the links between the boundary layer pattern with the performances of the foil remains unclear. Nevertheless, an increasing interest on boundary layer at high angle of attack can be noticed in order to predict the type of hysteretic loop that may occur [5] or to quantify the unsteady oscillatory flow in the near wake that produces pressure fluctuations as sources of hydroacoustic noise [6]. In addition, experiments have been performed to explore unsteady separating boundary layer [7] or the influence or laminar separation and transition on hysteresis on particular airfoil [8] but in these few references no systematic study of the effect of thickness is performed. The present work proposes such an attempt and with this aim, flows on three NACA symmetric foils (15%, 25% and 35% of relative thickness) are presented and detailed. The present study is a preliminary work of a major global VIV project in order to quantify the thickness effects of foils on the topology of the vortex shedding characterized by a predominant frequency persisting at high Reynolds.

2 Experimental Set Up and Measurements

The experiments have been conducted in the hydrodynamic tunnel of the French Naval Academy. This facility is fitted with a 1 m long and $0.192*0.192\,\mathrm{m}^2$ square cross test section, in which a maximum velocity of $15\,\mathrm{m\,s}^{-1}$ can be achieved. The turbulence intensity upstream at the entrance of the test section is 2%. The three designed foils are two-dimension symmetric profiles with relative maximum thickness of 15%, 25%, 35% located at 25% from the leading edge. The experiments have been performed on 100 mm chord length and 192 mm span length hydrofoils to a range of Reynolds number based on the chord length of $0.5\times10^6 < \mathrm{Re} < 1.3\times10^6$. The blockage ratios defined as t/H (H is the height of the test section, and t the maximum thickness of the foil are respectively 0.078 for the NACA0015 and 1.92 for the NACA0035. The draft of the experimental configuration is shown on Fig. 1.

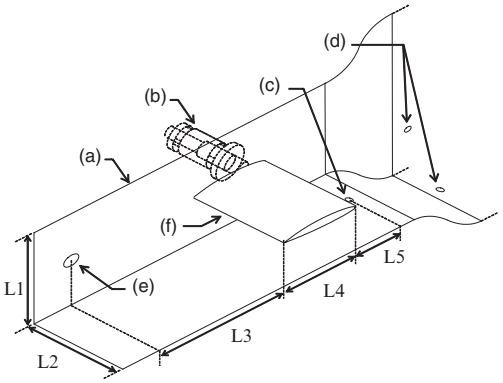

(a) Back wall of the vein
(b) Force balance
(c) Downstream pressure tap
(d) Upstream pressure taps
(e) Acoustical pressure sensor
(f) Profile
$L_1 = L_2 = 192$mm
$L_3 = 625$mm
$L_4 = 100$mm
$L_5 = 225$mm

Fig. 1 Experimental set up

Lift and drag measurements have been performed using a resistive gauge hydrodynamic balance calibrated in our laboratory. The mean and rms values have been performed from 30 s test measurements realized at 1,830 Hz. The determination of hydrodynamic parameters has been performed for $0° < a < 35°$ and the maximum range for the balance is 0–180 daN for the lift and 0–17 daN for the drag force.

To characterize the structure of the boundary layer that develop on the hydrofoils, detailed velocity measurements have been performed using a refined spatial grid. Two components, three beams, LDV Dantec Dynamics System was used to measure normal and tangential velocity components in water seeded with micron size particles of Iriodine. The dimensions of the probe volume are 0.8 mm in spanwise direction and 0.05 mm in vertical and longitudinal directions. Velocity measurements are performed in the boundary layer from the leading to the trailing edge ($0 < x/c < 1$) and a remote mechanical positioning system with a minimum translation step of 10 μm was used to obtained a cartography around the hydrofoil along a curvilinear map (x,y). For the boundary layer measurements the time histories were registered with 20,000 to 8,000 samples acquired in the range of 20 to 60 s corresponding to the mean data rates of 1,000 to 130 Hz. These parameters are sufficient to obtain the mean and rms values of the velocity with an uncertainty of 1% and 1.5% respectively.

The plan of measurements is located at a quarter the spanwise length and at each station x/c measurements are performed on the wall normal from the outer region of the boundary layer. The grid, refined in the near wall region (50 μm between grid points) allows the determination of the mean velocity gradient with a good accuracy. The grid represents 15 normal lines from the leading to the trailing edge with about 70 points per line. To locate the laminar/turbulent transition with an accuracy of 2% of x/c, the grid has been refined locally in x direction. The closest point corresponds to as mean distance to the wall of $y/c = 5 \cdot 10^{-4}$. In the chord wise direction, measurements are provided every $x/c = 0.1$ for every $y/c = 5 \cdot 10^{-4}$. The typical grid is shown Fig. 2.

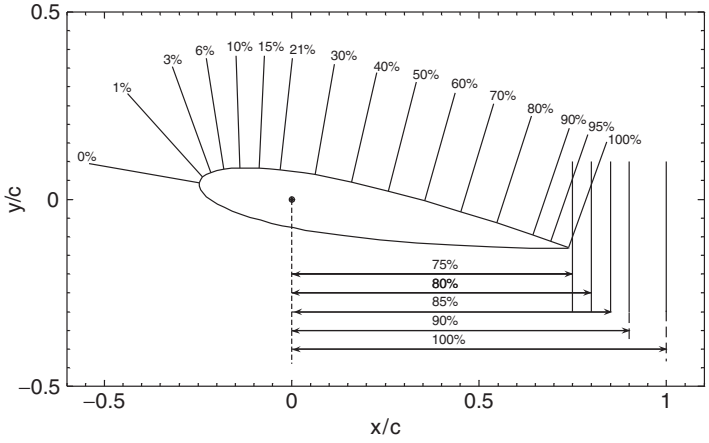

Fig. 2 Measurement locations

Concerning unsteady separated states, a spectral analysis has been conducted in the shear layer downstream and in the wake of the foils using a maximum data rate of 2,000 Hz for 400 s samples leading to a spectral resolution of 0.25 Hz. Spectral analysis of the vertical velocity component are provided by the Fast Fourier Transform method on the randomly sampled signals.

3 Thickness Effects on Global Parameters

3.1 Lift and Drag Measurements

Classic behaviour of both lift and drag coefficients is observed in Fig. 3 for low angles of attack. An abrupt loss of lift, characteristic of the stall, is observed on the NACA 0015 and on NACA 0025 for higher angles. For the two thinnest profiles the lift behaviour is linear for small values of the angle of attack. For the thickest one, a screen effect delays the establishment of the lift, leading to a non linear behaviour for small angles of attack indicated by (a) on Fig. 3. It can be noticed that the linear range of angles of attack increases with the thickness of the profile. Thus angles limiting the linear behaviour are 7°, 13° and 16° respectively on the three profiles. Stall appears for angles of 21°, 33° and 40°.

The evolution of the drag coefficient remains classical: for low incidences the effect of thickness is visible by an increase of the drag coefficient with increasing thickness. On these curves the stall is linked with a violent increase of the drag coefficient except for the NACA0035 for which stall appears at larger incidences. The effect of thickness introduces a decrease the slop of the lift coefficient with increasing thickness. This effect is characteristic of thick profiles.

3.2 Hysteretic Behaviour and Fluctuating Efforts

For the NACA0015 and NACA0025 profiles an abrupt loss of lift, characteristic of the stall, is observed for an angle of attack of 21° and 33° respectively.

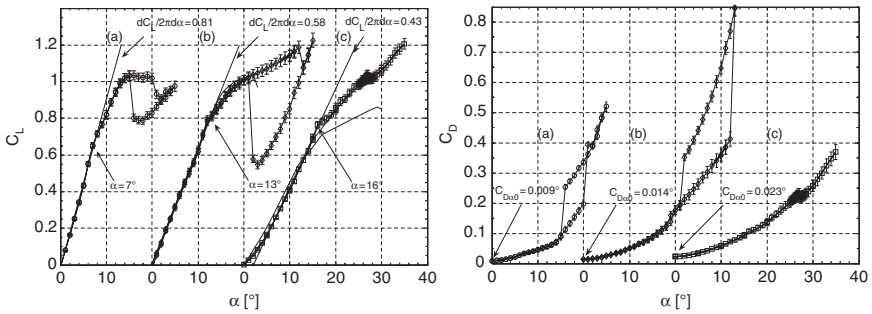

Fig. 3 Lift and drag coefficients for the three profiles

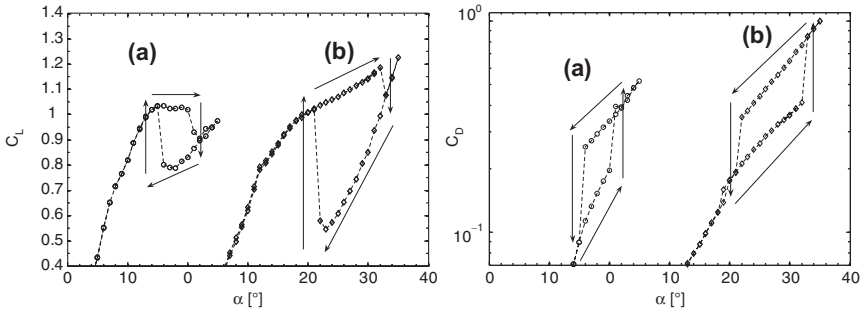

Fig. 4a Zoom of the hysteretic behaviour of lift (*left*) and drag (*right*) coefficients for NACA0015 (**a**) and NACA0025 (**b**)

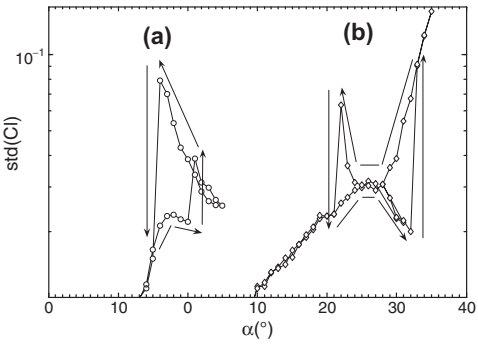

Fig. 4b Zoom of the hysteretic behaviour of fluctuating efforts lift (*left*) and drag (*right*) for NACA0015 (**a**) and NACA0025 (**b**)

For flow reattachment the angle of attack must be drastically reduced and are respectively 15° and 23°. This behaviour is illustrated in Figs. 4a and 4b where the hysteresis loops have been underlined by arrows following the cycle of the lift coefficient. In fact, the cycle provides an upper and lower branches characterized by two different states of the flow. The starting point for the flows along the increasing angle branch is an attached flow (called State I), whereas it is a massively separated flow for the flows along the branch corresponding to the decreasing angle (called state II). Corresponding boundary layer pattern has been observed and described in detail in Section 4.2. This phenomenon is not observed on the thickest profile in the range of our investigation. We were obliged to increase the angle of attack up to 40° in order to observe a similar phenomenon. The rms values of lift and drag coefficients at the stall angle show that the hysteretic behaviour is associated with an abrupt increase of fluctuations of forces. This increase of fluctuating part is associated with the unsteady component of hydrodynamic coefficients.

3.3 Turbulent Boundary Layer States

For each point of measure 20,000 samples have been validated during a maximum of 60 s (corresponding to the near wall locations). This has been proven sufficient after having performed successive tests to measure the mean and the *rms* values of the *u* and *v* velocity components with a very good convergence and repetitiveness of the processing. According to the previous refined grid, a survey of the distribution of mean tangential and normal velocity components is presented. Firstly, our goal was to characterise the boundary shape parameters on a Naca0015, 25 and 35 hydrofoils. Velocity profiles were numerically integrated to compute the displacement, δ_1, momentum, δ_2 and energy, δ_3, thicknesses from which shape factors H_{12} and H_{23} are deduced. The following formulas are applied:

$$\delta_1 = \int_0^{\delta} \left(1 - \frac{u}{U_e}\right) dy,\ \delta_2 = \int_0^{\delta} \left(1 - \frac{u}{U_e}\right) \frac{u}{U_e} dy,\ \delta_3 = \int_0^{\delta} \left(1 - \frac{u^2}{{U_e}^2}\right) \frac{u}{U_e} dy$$

$$H_{12} = \frac{\delta_1}{\delta_2},\ H_{23} = \frac{\delta_2}{\delta_3}$$

U_e represents the external velocity on the normal line. In our case this velocity is the maximum velocity measured at the location.

Shape factors are presented Fig. 5 versus normalized chord length. It can be observed that the thickness effect is associated with an increase of the length of the laminar region near the leading edge which grows from less than 10% on the NACA0015 to 30% on the NACA0035. At the end of this area the shape factor increases to reach a value of 3 to 4 just before the occurrence of the transition. After the transition, the value of H_{12} remains constant and equal to 1.6. This value increases near the trailing edge when the flow reaches conditions of separation. The

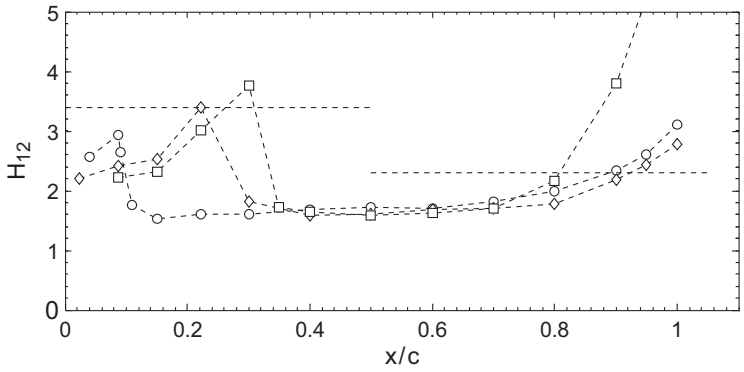

Fig. 5 Shape factors for the three profiles, $\mathrm{Re} = 5{\cdot}10^5$, $\alpha = 10°$, ○ NACA0015, ◇ NACA0025, □ NACA0035

constant value of H_{12} is larger than the value generally observed for turbulent boundary layers (1.4). It must be noticed that this value depends rigorously of the Reynolds number [9]. Near the trailing edge the shape factor is lower than 3 on the two thinner profiles and is greater than 4 on the third where separation is observed. These values are consistent with the threshold values proposed by Bradshaw [10].

To check the self similarity and to quantify the thickness effect of the foils on the boundary layer, mean velocity profiles with inner variables are presented. Inner variables are classically defined as $y+$ for the normal position and $u+$ for the tangential component of the velocity respectively given by:

$u^+ = A \log y^+ + B$ with $y^+ = \frac{yu^*}{\nu}$ and $u^* = U_e\sqrt{\frac{C_f}{2}} = \sqrt{\frac{\tau_w}{\rho}}$, where τ_w is the wall shear stress. To determine the value of the shear stress velocity u^*, an efficient estimation of the skin friction is required. The friction has been determined using an experimental model based on the value of the integral quantities proposed by Ludwieg and Tillman in 1950 [11]:

$C_f = 0.246\frac{Re_{\delta 2}{}^{-0.268}}{10^{0.678H_{12}}}$, the values obtained with the model are in a good agreement with numerical results (boundary layer code 3C3D) and with the near wall velocity gradients. Figure 6 the velocity profiles using scaling law are reported for the three foils at different locations on x/c. It can be noticed that the slopes of the profiles in the logarithmic area are quite far from the classical value 5.75 obtained for turbulent boundary layers on flat plates. This is due to the non equilibrium boundary layer condition due to the low Reynolds number effects. Moving downstream, the velocity profiles in wall coordinates deviate significantly from the standard log-law and it can be noticed that the thickness effect pronounce this trend. Despite the Reynolds effect, the thickness effect is only characterized here by the shape of the wake region. For the locations x/c near the trailing edge, the wake area can be described by a second law proposed by Coles [12] for $y^+ > 100 :\ u^+ = f\left(y^+\right) + \frac{\Pi}{\kappa}\omega\left(\frac{y}{\delta}\right)$ where δ is the boundary layer thickness. With the non equilibrium layers the wake law can be used according the evolution of Π with x/c and the different value of κ [13]. The hypothesis of a universal wake function is reported Fig. 6 for the three profiles at different station x/c. The thickness effect is then characterized by a deviation of the wake law accentuated for the two thicker profiles.

4 Unsteady Separated Flow

4.1 Strouhal Number

When incidence is increased over 20°, an organized motion due to the regular vortex shedding appears. This shedding is characterized by a predominant frequency f. The evolution of von Karman instability is shown for the three profiles on Fig. 7. The establishment of the instability is associated with an increase of maximum amplitude and a decrease of the frequency. For NACA0015 the frequency evolves linearly but for the two thicker profiles if the behaviour remains linear, two different slopes can

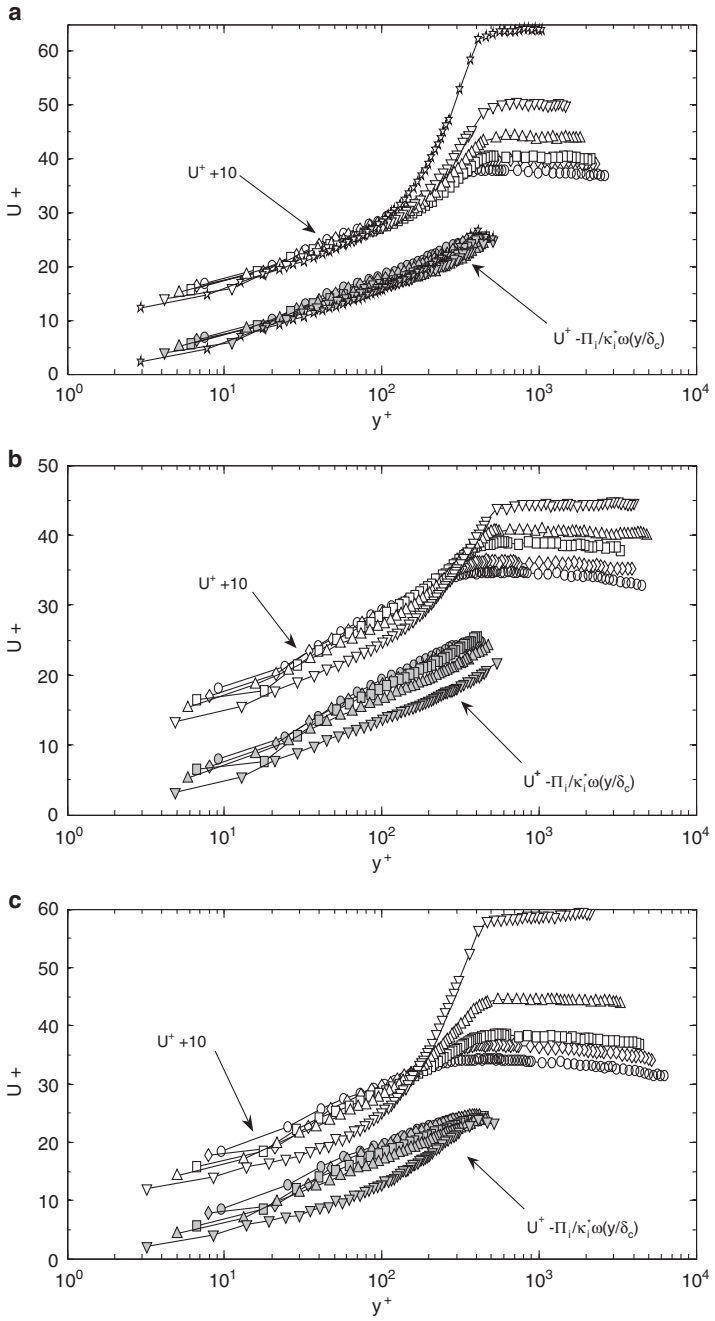

Fig. 6 Velocity profiles with inner coordinates and associated wake laws, $\alpha\Theta = 10°,\ 5\,\mathrm{m\,s^{-1}}$, (**a**) NACA0015, (**b**) NACA0025, (**c**) NACA0035

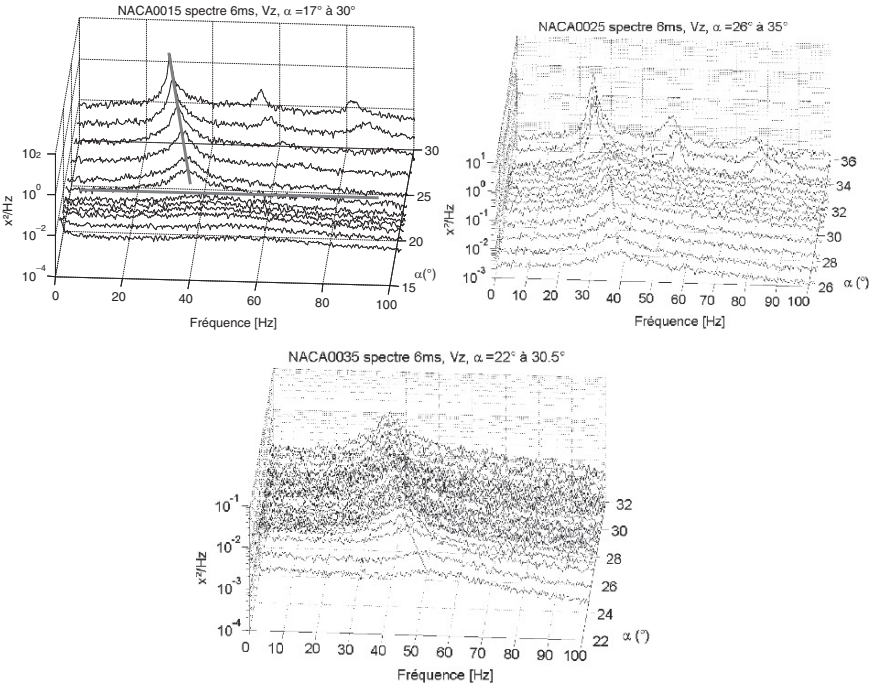

Fig. 7 Frequency spectrum of the vertical velocity in the shear layer for the three profiles

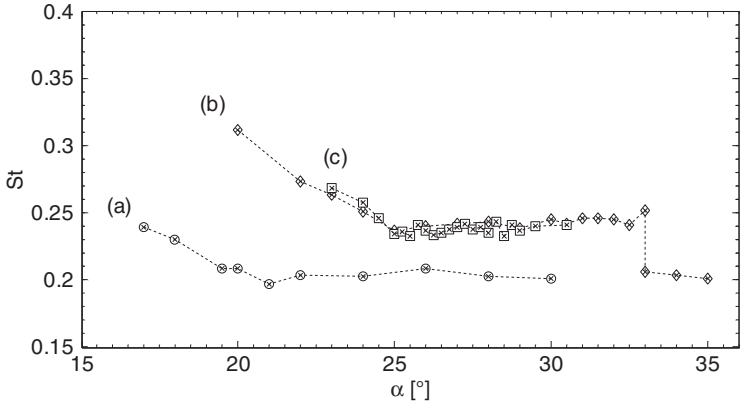

Fig. 8 Strouhal number versus incidence for the three profiles

be observed. These different evolutions are characterized by two values of Strouhal number, based on the projected area of the foil defined as $\mathrm{St} = \mathrm{c}\ \sin\alpha\ \mathrm{f}/\mathrm{U}$.

This number is reported versus the angle of attack for each profile on Fig. 8. Two states of the flow which characterized by two values of St (0.3 in state I and 0.2 in state II) are shown. The transition between the two states is characterized by a

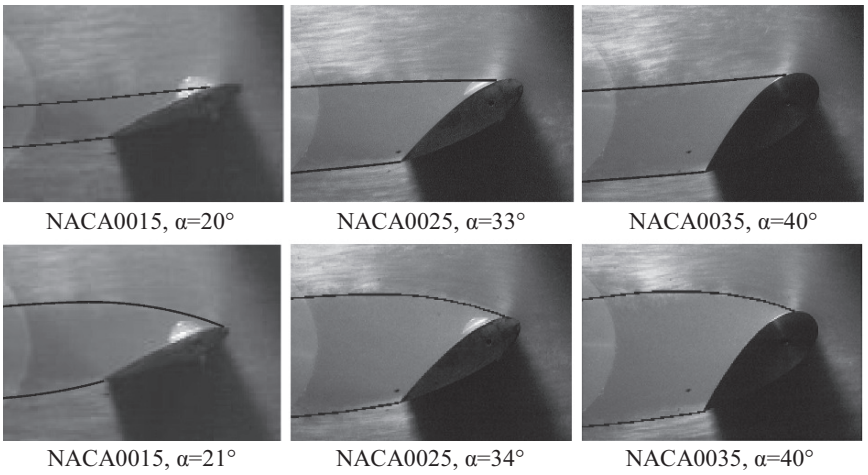

Fig. 9 Flow visualization of the two states I and II for the three profiles

jump of the Strouhal value. In state I, the flow is partially attached in the vicinity of the leading edge when in state II, the flow detaches at the leading edge (stall mechanism). This sketch is illustrated Fig. 9. This figure shows the flow patterns that characterize the two branches of hysteresis loop. This behaviour is observed on the three profiles but experimental range is not large enough to measure precisely the value on NACA0035.

When the incidence angle of the foil is increased, the separation point appears near the trailing edge and moves progressively towards the leading edge (steady state configuration). A vortex shedding appears as it is observed through the spectral analysis, and the shear layer at separated point is affected by Kelvin Helmotz instability. This instability, forced by the periodic vortex shedding, lead to an oscillation of the stagnation point and further an oscillation of the separation point. The non linear interaction between these two instabilities seems to be responsible of the coexistence of the state I and II [13]. A second mechanism that can lead to the static stall (transition from state I to state II) is linked with the value of the maximum speed near the leading edge. A comparison between the flow patterns on the three profiles shows that:

(i) For the same incidence angle the maximum velocity observed on the three profiles is a decreasing function of the relative thickness.
(ii) Just before the transition the maximum velocity observed on the three profiles are equal.

Thus it seems that for a fixed Reynolds number a velocity threshold that can't be overcome by the flow exists. The measurements realized for the two flow states are presented in the next paragraph.

4.2 *Boundary Layer State During Hysteresis*

On the Naca0015 boundary layer measurements have been performed in the range of angle where hysteretic behaviour is observed at the same incidence angle for the two flow states I and II. The chosen incidence angles are 16° and 20°. The same measurements have been performed on NACA0025 for the two specific states at $\alpha = 25°$. When the incidence angle of the foil is increased two phenomena occur simultaneously on the foil. The transition point and the detachment points move progressively toward the leading edge and the distance between the two points decreases. The detachment point behaves more and more unsteady.

As it is observed, Figs. 10a and 10b, for the thinner profile the transition to the state II is characterized by an abrupt modification of the localisation of the detached point $x/c = 0.45$ for state I and $x/c = 0.023$ for state II. For NACA0025 profile, the magnitude of the displacement of the detached point is less pronounced ($x/c = 0.35$ for state I and $x/c = 0.043$ for state II). To conclude, the thickness of the profile tends to increase the thickness of the boundary layer at low angle of attack instead of at stall, the magnitude of the detached point raising is attenuated leading to a less decrease of the lift. This effect corroborates the well known stall mechanism of the thick profile.

On Fig. 11 the local velocity on the suction side is presented versus x coordinate as a Cp value: $Cp = 1 - \left(\frac{U_e}{U_{ref}}\right)^2$. It can be seen that for the two conditions that prevail just before stall occurrence the maxima of the velocity (corresponding to the

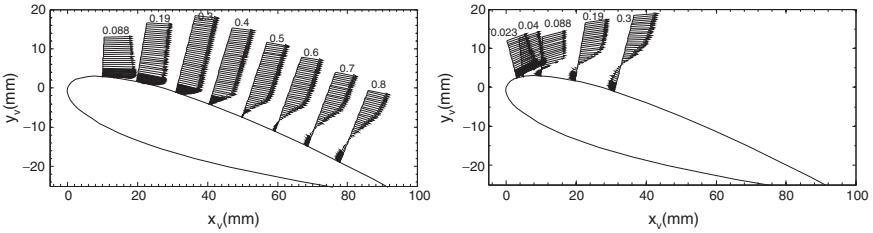

Fig. 10a Velocity profile for NACA0015 at 16° corresponding to state I (*left*) and state II (*right*)

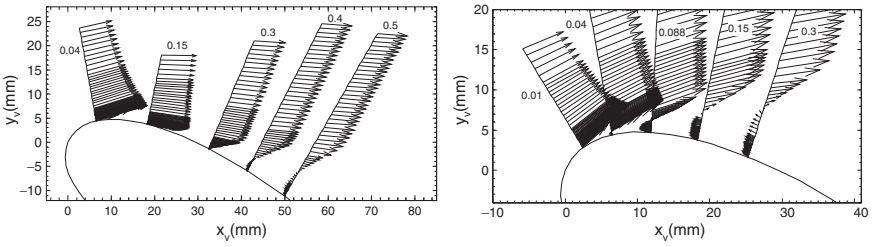

Fig. 10b Velocity profile for NACA0025 at 25° corresponding to state I (*left*) and state II (*right*)

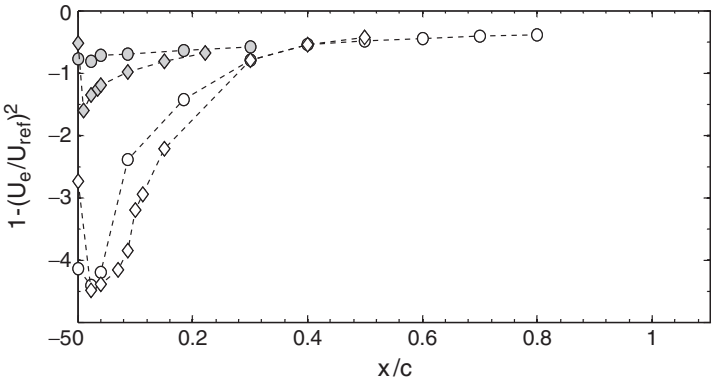

Fig. 11 Velocity on the two profiles (suction side) just before (open symbols) and just after (solid symbols) stall occurrence ○: NACA0015 $\alpha = 16°$ ◇: NACA0025 $\alpha = 25°$

Cp minimum) are equal for the two profiles. After stall occurrence (corresponding to the state II), the thickness effect induces a larger maximum of the velocity on the thicker profile.

5 Conclusions

This experimental work realized on three symmetrical NACA profiles of 15%, 25% and 35% relative thickness have shown that:

Above about 10% thickness the lift coefficient of the profile decreases when the thickness is increased. The hysteretic behavior of the profile at stall is delayed when the thickness is increased, this phenomenon is correlated with a modification of the flow state linked with the position of the detachment point which is forced by the establishment of Karman instabilities. Concerning the unsteady separated flow at high angle of attack, the thickness effect is associated with a modification of the establishment of the Karman street. Indeed, as it is observed through the spectral analysis for the thinner profile, the frequency evolves linearly but for the two thicker profiles if the behaviour remains linear, two different slopes can be observed.

The thickness of the profile tends to increase the thickness of the boundary layer at low angle of attack instead of at stall, the magnitude of the detached point raising is attenuated leading to a less decrease of the lift. The boundary layers that develop on the three profiles are turbulent even if they have not reach their equilibrium state with establishment of the self similarity. The effect of the adverse pressure gradient implies the use of two velocity laws (near wall logarithmic law and wake law) that can be unified using the Coles law for the velocity profiles close to the detachment point. The thickness effect is then characterized by a deviation of the wake law accentuated for the two thicker profiles.

References

1. Thwaites, B., Incompressible aerodynamics, an account of the theory and observation of the steady flow of incompressible fluid past aerofoils, wings and other bodies. Dover, 1960.
2. Na, Y. and Moin, P., Direct numerical simulation of a separated turbulent boundary layer, J. Fluid Mech., 370, 1998.
3. Yang, Z. and Voke, P., Large eddy simulation of boundary layer separation and transition at a change of surface curvature, J. Fluid Mech., 439, 2001.
4. Marusic, I. and Perry, E., A wall-wake model for the turbulence structure of boundary layers, J. Fluid Mech., 298, 1995.
5. Mittal, S. and Saxena, P., Prediction of hysteresis associated with the static stall of an airfoil, AIAA J., 38(5), 2000.
6. Bourgoyne, D.A., Ceccio, S., Dowling, D., Jessup, S., Park, J., Brewer, W., and Pankajakshan, R., Hydrofoil turbulent boundary layer separation at high Reynolds numbers, 23rd Symposium on Naval Hydrodynamice, Val de Reuil, France 2000.
7. Lurie, E.A., Keenan, D.P., and Kerwin, J.E., Experimental study of an unsteady separating boundary layer, AIAA J., 36(4), 1998.
8. Mueller, T., The influence of laminar separation and transition on low Reynolds number airfoil hysteresis, J. Aircraft, 22(9), 1985.
9. Cousteix, J., "Turbulence et couche limite" Aérodynamique, Editions Cepadues, 1989.
10. Bradshaw P., "The turbulence structure of equilibrium boudary layers", J. Fluid Mech., 29:625–645, 1967.
11. Ludwieg, H., and Tillman, W., Investigation of the wall-shearing stress in turbulent boundary layer, NACA Technical Memorandum, 1285, 1950.
12. Coles, D., "The law of the wake", J. Fluid Mech., 1:191–226, 1956.
13. Hoarau Y., Braza M., Ventikos Y., Faghani D., and Tzabiras G.: "Organized modes and the three dimensional transition to turbulence in the incompressible flow around a NACA0012 wing", J. Fluid Mech., 496:63–72, 2003.
14. Hoarau, Y. and Braza, M., Simulation et contrôle d'un écoulement fortement décollé autour d'un profil d'aile, 39 ème colloque d'aérodynamique appiqué AAAF 2004-04-08.